Vegetation Identification in Hyperspectral Images of Cartagena City Using the Haar Wavelet Transform

Gabriel Elías Chanchí Golondrino[1], Manuel Alejandro Ospina Alarcón[2], Manuel Saba[3]
Faculty of Engineering-Systems Engineering Program, University of Cartagena, Cartagena, Colombia[1, 2]
Faculty of Engineering-Civil Engineering Program, University of Cartagena, Cartagena, Colombia[3]

Abstract—**Hyperspectral imaging is one of the most widespread remote sensing techniques in earth observation, corresponding to images with high spectral and spatial resolution that enable material detection through the identification of their spectral signature. A key challenge in hyperspectral imaging is the definition of novel and efficient computational methods that contribute to reducing computational cost while maintaining the efficacy and precision in material detection provided by methods such as correlation or machine learning. This study aims to propose a new efficient method for vegetation detection in hyperspectral images based on the similarity between the approximate and detailed components of the Haar wavelet transform of the vegetation spectral signature, with respect to the components of the pixel to be classified in the image. For the development of the present investigation, five methodological phases were defined: P1. Selection of sample pixels for vegetation and other materials; P2. Determination of the characteristic vegetation pixel; P3. Implementation and evaluation of the method with vegetation and non-vegetation pixels; P4. Deployment of the method on the reference hyperspectral image; P5. Comparative evaluation of the proposed method against the correlation method. As a result of this research, a novel computational method for vegetation identification in hyperspectral images was proposed, leveraging the similarity of wavelet transform components. This method demonstrated comparable detection efficacy to the correlation method and proved to be approximately 5% more efficient in the detection process. The proposed method can be suitably integrated into hyperspectral image-based environmental monitoring systems, particularly where images are of considerable size and more efficient methods are required.**

Keywords—Vegetation detection; hyperspectral images; remote sensing; wavelet transform; earth observation

I. INTRODUCTION

Remote sensing is a set of techniques that make it possible to observe the Earth's surface without direct contact; sensors on satellites [1], [2], airplanes, drones, or ground-based instruments [3], [4] get electromagnetic energy reflected by different materials, such as visible, infrared, and microwave radiation [5]. These systems provide fast access to large areas and help lower the time and cost of ground measurements [3], [6].

This technology also gives access to information that humans cannot see directly, as it shows soil conditions, vegetation health, and atmospheric properties; such data supports better decisions in natural-resource management [7], [8]. Within remote sensing, hyperspectral imaging has become one of the most used techniques [9] because it includes many narrow spectral bands that let users distinguish materials with high precision [10], [11].

Unlike multispectral images, hyperspectral data cubes have many more bands and show the unique spectral signature of each surface material [12], [13]. A hyperspectral image is a three-dimensional data cube [14], [15], where the first two dimensions show spatial location and the third shows reflectance as a function of wavelength [16], [17].

Hyperspectral imaging plays an important role in environmental and agricultural studies. For example, it helps identify tree species and supports biodiversity planning [18]. It lets researchers detect salt crusts in estuaries and follow climate-related patterns [19]. It also helps monitor vegetation changes through time using multisensor data and clustering methods [20].

Other applications include mapping biodiversity with NDVI and autoencoders [21], detecting microplastics [22] and supporting the management of water resources [23]. In agriculture, hyperspectral images help detect diseases early [24], classify multiple crop types [25], [26], and show product quality in a non-destructive way [27]-[29]. They also support soil and crop characterization tasks [30], [31].

However, hyperspectral images bring several challenges. They contain large volumes of redundant data, which need dimensionality-reduction methods [32], [33]. Machine learning and deep learning methods often get good results but need big annotated datasets, high processing power, and complex architectures [34], [35]; these requirements make them difficult to use in real-time environmental monitoring.

For vegetation detection, correlation-based approaches [36] and learning-based methods [20] seem to be the most common choices. Still, they leave open questions about efficiency, data needs, and operational cost. Because of this, there is a need for solutions that keep detection accuracy while cutting computational load.

Building on this, the present study uses the similarity between the approximate and detailed components of the Haar wavelet transform to detect vegetation in hyperspectral images. The Haar transform provides a simple structure that lets users break a signal into low- and high-frequency components [37], [38], which can show features relevant for material discrimination [39], [40].

This work uses open-source Python libraries (spectral, PyWavelets, numpy, pandas, matplotlib) to evaluate the method with 100 sample pixels (vegetation and non-vegetation). After estimating the detection threshold, the method is applied to a hyperspectral image from Cartagena City (750×850 pixels, 380 bands) and is compared to the correlation method.

Beyond performance, this method can help researchers and practitioners who need efficient tools for large-scale environmental monitoring systems. The use of open-source libraries makes the method easier to replicate and adopt in academic and commercial settings.

Despite the wide range of applications of hyperspectral imaging, vegetation detection still relies predominantly on correlation-based approaches or machine learning models that require large annotated datasets and high computational cost. These methods are accurate but often inefficient when processing large hyperspectral scenes, which limits their integration into operational environmental monitoring pipelines. Consequently, there is a need for computationally efficient alternatives that preserve detection capability while reducing processing time.

To address this gap, this study proposes a new method for vegetation detection based on the similarity between the approximate and detailed components of the Haar wavelet transform of the vegetation spectral signature. The main contributions of this work are:

1) A wavelet-based vegetation detection strategy that reduces dimensionality while preserving spectral structure;
2) A threshold estimation procedure based on combined similarity metrics; and
3) A comparative evaluation against the widely used correlation method in terms of detection accuracy and computational efficiency.

The remainder of the study is organized as follows: Section II presents the literature review and problem statement. Section III describes the methodological phases considered for the development of this research. Section IV presents the results obtained in this study, including the calculation of the approximate and detailed components of the characteristic vegetation pixel; the implementation and evaluation of the method with vegetation and non-vegetation sample pixels to identify detection thresholds; and the deployment of the method on the reference hyperspectral image, comparing its effectiveness and efficiency with the correlation method. Section V presents a discussion of the results, analyzing them in relation to the reviewed literature. Finally, Section VI outlines the conclusions derived from this research.

II. Literature Review and Problem Statement

Unresolved questions are related to the need for very large annotated datasets. The reason is that collecting and labeling such datasets is costly and often unfeasible in many agricultural contexts.

The study [18] demonstrates hyperspectral imaging for identifying tropical tree species. It is shown that the approach is effective at the local scale, but unresolved issues include transferability, since the method relies on curated spectral libraries that are difficult to build for large and diverse ecosystems.

In [20], the authors introduce a multi-sensor framework for detecting vegetation changes. It is shown that temporal dynamics can be effectively captured. However, unresolved questions arise from operational complexity and costs, because the approach requires repeated multi-temporal acquisitions.

The study [21] combines convolutional autoencoders with vegetation indices to map biodiversity. It is shown that detailed and high-resolution outputs can be obtained, but unresolved questions include the need for intensive computational resources and large labeled datasets, which limit its applicability in practice (see Table I).

TABLE I. Summary of Recent Studies on Hyperspectral Vegetation Analysis

Ref.	Year	Features		
		Method	***Application***	***Limitations***
[32]	2009	General hyperspectral image processing	Foundational techniques	High dimensionality and redundancy
[19]	2014	Hyperion imagery for salt crust mapping	Estuarine monitoring	Dependence on atmospherics correction models
[25]	2015	Non-destructive analysis of agricultural products	Stored food quality	Expensive hardware and limited scalability
[22]	2020	Deep learning on microscopic hyperspectral data	Microplastic detection	Limited generalization to field data
[23]	2021	Multi/hyperspectral analysis for water quality	Aquatic environments	Computational bottlenecks for real-time use
[26]	2021	Deep learning for agricultural hyperspectral data	Crop disease detection	Requires large labeled datasets
[18]	2022	Hyperspectral imaging of tropical trees	Biodiversity analysis	Reliance on curated spectral libraries
[20]	2024	Multi-sensor change detection	Vegetation monitoring	High operational complexity and cost
[21]	2024	Autoencoders vegetation indices	Biodiversity mapping	Intensive computational resources

The above analysis of the literature review allows to argue that it is appropriate to conduct a dedicated study on computationally efficient vegetation detection methods.

Limitations presented in Table I highlight the need for more efficient spectral processing techniques that can maintain analytical accuracy while reducing the time and cost associated with hyperspectral data interpretation.

The approach proposed in this study, based on Haar wavelet decomposition, directly addresses these gaps by offering a balanced, computationally efficient alternative for vegetation detection.

III. METHODOLOGY

The proposed vegetation detection method is designed as a sequential and reproducible workflow. Although the detailed description is presented through five methodological phases, the overall procedure can be summarized as follows: selection of representative vegetation and non-vegetation pixels; construction of a characteristic vegetation spectral signature; wavelet-based decomposition of spectral data; similarity analysis and threshold determination; and pixel-wise deployment of the method on the full hyperspectral image, followed by a comparative evaluation with the correlation method. The complete workflow and its individual phases are detailed below and summarized in Fig. 1.

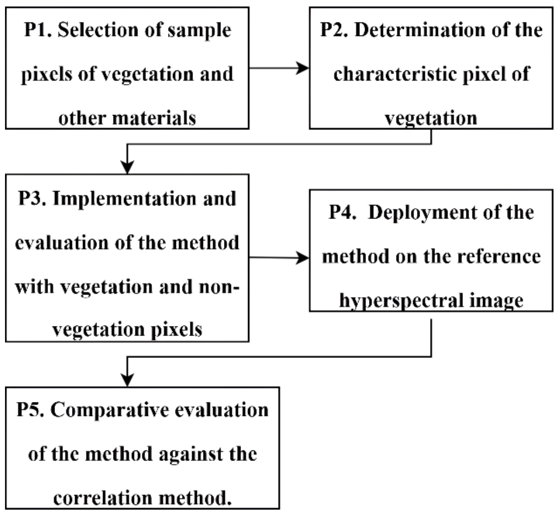

Fig. 1. Considered methodological phases. The diagram summarizes the complete workflow of the proposed vegetation detection approach.

For the development of this research, five methodological phases were defined as follows in Fig. 1. This diagram summarizes the workflow of the proposed approach, allowing one to understand the sequence of processes from data acquisition to vegetation detection and performance evaluation:

- P1. Selection of sample pixels representing vegetation and other materials.
- P2. Determination of the characteristic vegetation pixel.
- P3. Implementation and evaluation of the method using vegetation and non-vegetation pixels.
- P4. Deployment of the method on the reference hyperspectral image.
- P5. Comparative evaluation of the method against the correlation method.

In Phase 1 of the methodology, using a hyperspectral image of the city of Cartagena, Colombia, with 750 x 850 pixels and 380 reflectance bands per pixel, a set of 50 sample pixels corresponding to vegetation and 50 pixels corresponding to other materials were visually inspected and selected. This process aimed to obtain the spectral signature of vegetation and evaluate the method with vegetation and non-vegetation pixels.

The sampling strategy was designed to capture representative spectral signatures while avoiding oversampling effects that may reduce separability in threshold-based similarity analysis.

Once the vegetation and non-vegetation pixels were selected, Phase 2 involved calculating the characteristic vegetation pixel by averaging the normalized reflectance values of the 50 vegetation pixels band by band.

In Phase 3 of the methodology, the determination of the approximate and detailed components of the Haar wavelet transform for the characteristic vegetation pixel was initially performed using Eq. (1) and Eq. (2). The approximate components of the Haar wavelet transform are given by Eq. (1):

$$A_i = \frac{r_{2i-1} + r_{2i}}{\sqrt{2}}, i = 1,2,\ldots,190 \quad (1)$$

where, Eq. (1) defines the approximate components Ai of the Haar wavelet transform, which are derived from an array of 380 values corresponding to the normalized reflectance associated with the 380 bands of the characteristic vegetation pixel or spectral signature ($R = [r_1, r_2, r_3 \ldots, r_{380}]$). It is important to note that, since the Haar wavelet transform operates on consecutive pairs, the array of approximate components Ai consists of a total of 190 elements, equivalent to half of the 380 reflectance bands.

The detailed components of the Haar wavelet transform are expressed as Eq. (2):

$$D_i = \frac{r_{2i-1} - r_{2i}}{\sqrt{2}}, i = 1,2,\ldots,190 \quad (2)$$

Eq. (2) defines the detailed components Di of the Haar wavelet transform, which also begins with an array of 380 normalized reflectance values from the characteristic pixel and produces an array Di consisting of 190 values. This reduction occurs because, for the detailed component as well, the Haar transform operates on consecutive pairs.

Using the components obtained through Eq. (1) and Eq. (2), an iteration was performed over the 50 vegetation sample pixels and the 50 pixels representing other materials, calculating the approximate and detailed components of the wavelet transform for each pixel.

Through the use of Euclidean distance, a similarity percentage was determined for each component of each pixel, and a combined similarity percentage was calculated for both components.

The process aimed to identify the minimum combined similarity percentage with vegetation pixels and the maximum combined similarity percentage with pixels of other materials. These thresholds enable the assessment of potential overlap between the two, and in the absence of overlap, the detection or differentiation capability of the method can be established, along with the threshold to be considered for deploying the method on the entire reference image.

Phase 4 involved deploying the method on each pixel of the reference hyperspectral image (Once the vegetation detection threshold was identified in Phase 3). For each pixel, the wavelet transform components were obtained, and the similarity percentages for each component, as well as the combined similarity percentage were calculated. The combined percentage was then used to classify each pixel in the image as either vegetation or another material.

Additionally, in this phase, the number of pixels detected by the method was counted, and the percentage of pixels within the hyperspectral image corresponding to this count was calculated.

Finally, in Phase 5, the correlation method was implemented after detecting the reference thresholds, and both the number of vegetation pixels and the percentage corresponding to this pixel count were determined. This allowed for a comparison of the effectiveness of the proposed method with the correlation method.

Furthermore, in this phase, the computational efficiency of both methods was evaluated by performing a total of 20, 40, 60, 80, and 100 executions on a 50x50-pixel region of the image, each pixel containing 380 bands. For each method, the average execution time per number of runs and the total average time were calculated, enabling a comparison of the computational efficiency of one method relative to the other.

IV. Results

A. Selection of Pixels and Construction of a Characteristic Vegetation Signature

A hyperspectral image of Cartagena City with a resolution of 750 by 850 pixels and 380 spectral bands was used. From this image, 50 vegetation pixels and 50 non-vegetation pixels were manually selected for the evaluation phase.

Fig. 2 shows the RGB visualization of the hyperspectral scene with the manually selected vegetation (green) and non-vegetation (blue) pixels. This visual separation allows verifying that both classes are spatially well distributed across the study area, ensuring that the sample is suitable for computing representative spectral signatures and for estimating detection thresholds.

From the 50 manually selected vegetation pixels, individual spectral signatures were extracted to analyze their variability, as shown in Fig. 3. Fig. 3 shows the dispersion of reflectance values across the spectral bands, highlighting the natural spectral variability of vegetation within the study area.

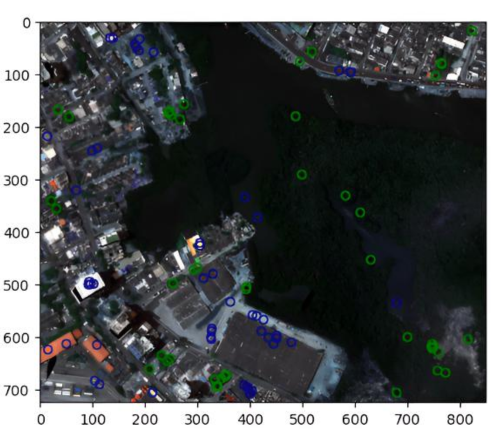

Fig. 2. Selected vegetation and non-vegetation pixels in the RGB rendering of the hyperspectral scene. The labeled samples provide the reference spectral signatures used to estimate similarity thresholds for vegetation detection.

To obtain a stable and representative reference for subsequent analysis, a characteristic vegetation pixel was computed by averaging the spectral signatures of the 50 vegetation samples. The resulting average spectrum, shown in Fig. 4, preserves the general spectral structure of vegetation, while reducing noise and sample-specific fluctuations.

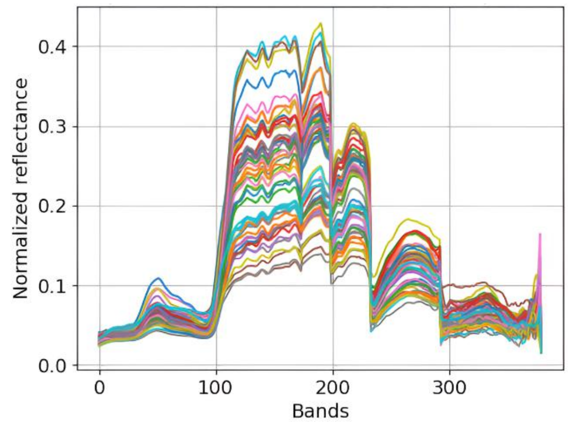

Fig. 3. Spectral signatures of the 50 selected vegetation pixels used to compute a representative reference signature.

The characteristic vegetation pixel shown in Fig. 4 plays a key role in the proposed method, as its wavelet components are compared with those of each pixel in the hyperspectral image (Fig. 1) to determine the presence of vegetation through a similarity analysis.

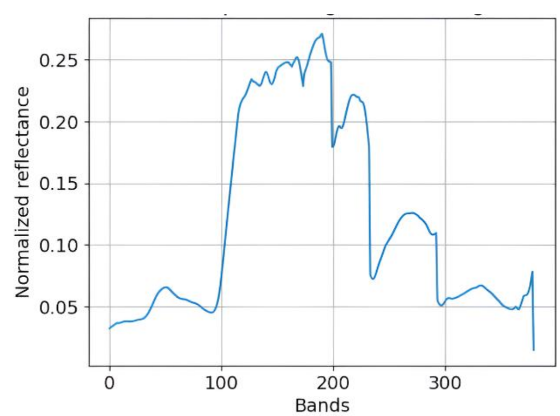

Fig. 4. Spectral signatures of characteristic vegetation pixel used for wavelet decomposition.

B. Wavelet Decomposition

Haar wavelet transform was applied to average (the characteristic) vegetation pixel shown in Fig. 4. This process generated two sets of coefficients: the approximate components (Ai) (see Fig. 5) and the detailed components (Di) (see Fig. 6), which are defined in Eq. (1) and Eq. (2), respectively.

Since the Haar transform operates by pairing consecutive reflectance values, each component contains 190 coefficients, corresponding to half of the original 380 spectral bands. The same transformation was then applied to all 100 sample pixels, including the 50 vegetation and 50 non-vegetation samples, using the characteristic vegetation pixel as the reference for similarity comparisons.

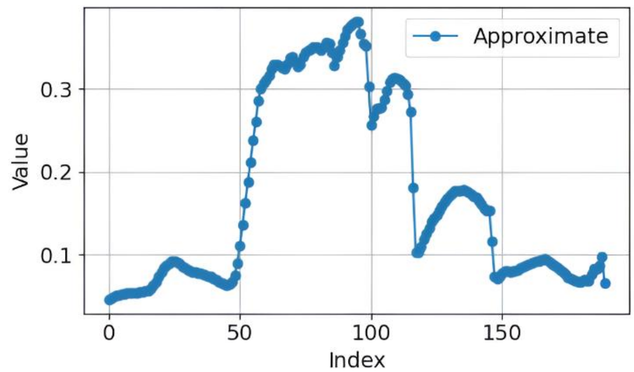

Fig. 5. Approximate component of the characteristic vegetation pixel. It represents the main trend of the vegetation signature after dimensionality reduction.

Fig. 5 shows the approximate component of the characteristic vegetation pixel. This component can be interpreted as a simplified representation of the original spectral signature, as it preserves the low-frequency information and captures the main spectral trend of vegetation while reducing data dimensionality.

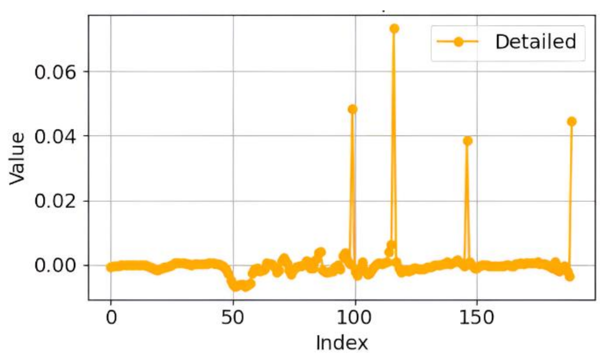

Fig. 6. Detailed component of the characteristic vegetation pixel. It captures local fluctuations between adjacent bands.

Fig. 6 shows the detailed component of the characteristic vegetation pixel. In contrast to the approximation, this component highlights high-frequency information by emphasizing local fluctuations between adjacent spectral bands, allowing the method to capture finer spectral variations relevant for discrimination.

C. Similarity Analysis

Once the transform components of the characteristic pixel were obtained, an iteration was performed over the 50 vegetation pixels and 50 pixels representing other materials to determine the approximate and detailed components for each pixel. Using these components, three similarities were calculated via Euclidean distance: the similarity between approximate components, the similarity between detailed components, and the weighted similarity between components. The results of the similarity analysis for the approximate and detailed components, comparing vegetation pixels with pixels from other materials, are presented in Fig. 7.

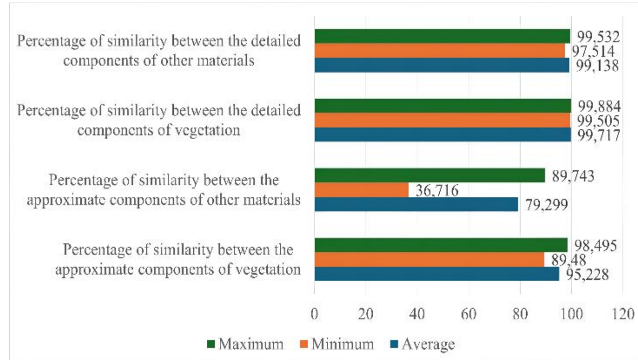

Fig. 7. Similarity percentages obtained for the approximate and detailed wavelet components when comparing vegetation and non-vegetation pixels.

As observed in Fig. 7, for the approximate component, the maximum similarity percentage obtained for non-vegetation pixels (89.743%) exceeds the minimum similarity percentage obtained for vegetation pixels (89.48%). This overlap indicates that the approximate component alone is not sufficient to reliably discriminate vegetation pixels. Similarly, for the detailed component, the maximum similarity percentage for non-vegetation pixels (99.532%) is higher than the minimum similarity percentage for vegetation pixels (99.505%), showing that this component by itself also fails to provide clear separation.

The results presented in Fig. 7 demonstrate that, although the coarse and fine components individually capture relevant spectral information, their isolated use does not allow for accurate vegetation discrimination. When both components are combined and greater weight is assigned to the fine component, the method becomes more sensitive to subtle spectral variations, allowing for more reliable classification and reducing detection errors.

D. Determination of Detection Thresholds

In light of the results presented in Fig. 7, where neither the approximate nor the detailed component alone provided sufficient discrimination, a weighted similarity measure was evaluated. The contribution of the detailed component was varied across different percentages (60%, 70%, 80%, 85%, 90%, 95%, and 98%), while the remaining weight was assigned to the approximate component.

The similarity results obtained for these weighted combinations, comparing vegetation and non-vegetation pixels, are presented in Fig. 8. This analysis allows identifying the weighting configurations that maximize the separation between both classes and serves as the basis for selecting an appropriate detection threshold.

As shown in Fig. 8, the only weighting configuration in which the minimum similarity percentage for vegetation pixels is lower than the maximum similarity percentage for non-vegetation pixels corresponds to a 60% contribution of the detailed component. For higher weight values, a clearer separation between both classes is observed.

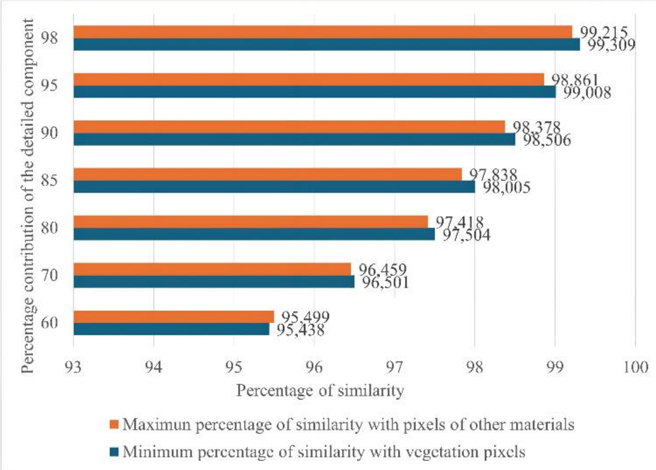

Fig. 8. Similarity percentages obtained for different weightings of the approximate and detailed wavelet components; supports the selection of the detection threshold.

It is noteworthy that the greatest differentiation between vegetation and non-vegetation similarities is achieved when the detailed component has a weight of 95% and the approximate component a weight of 5%, resulting in a percentage difference of 0.147%. Based on this result, the minimum detection threshold for identifying vegetation pixels was established at a similarity value of 99.008%, corresponding to a 95% contribution of the detailed component of the Haar wavelet transform.

Setting this threshold matters, because it turns the method into something practical and measurable. It defines a clear decision line that helps distinguish vegetation from other materials with confidence. The results also show that the Haar based decomposition can create thresholds with very little uncertainty, which is important for building scalable systems that rely on automated classification in environmental monitoring.

E. Large-Scale Deployment and Comparative Evaluation

Using the detection threshold of 99.008% (Fig. 8), the proposed method was deployed across the entire hyperspectral image (Fig. 1) of Cartagena City (750 × 850 pixels, 380 bands).

As shown in Fig. 9, for each pixel in the image, the approximate and detailed components of the wavelet were calculated, similarity scores were calculated with respect to the characteristic vegetation pixel, and a final classification into vegetation or non-vegetation was made.

The implementation was carried out exclusively with open-source Python libraries (spectral, PyWavelets, numpy, pandas, and matplotlib).

As a result, the method determined that 42.95% of the hyperspectral image corresponds to vegetation pixels. Fig. 9 presents the vegetation map generated by the proposed method, where detected vegetation areas are highlighted in blue, visually demonstrating the capability of the Haar wavelet transform measure to discriminate vegetation from other materials.

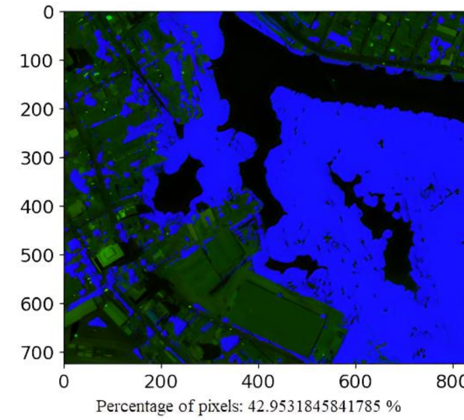

Fig. 9. Vegetation detection method applied to the entire hyperspectral image; final classification is performed.

To evaluate the performance of the proposed method, the traditional correlation-based approach was also applied to the same hyperspectral image (Fig. 1), once its corresponding detection threshold was defined. Fig. 10 illustrates the deployment of the correlation method across the entire scene, while Table II summarizes the vegetation detection results obtained with both techniques.

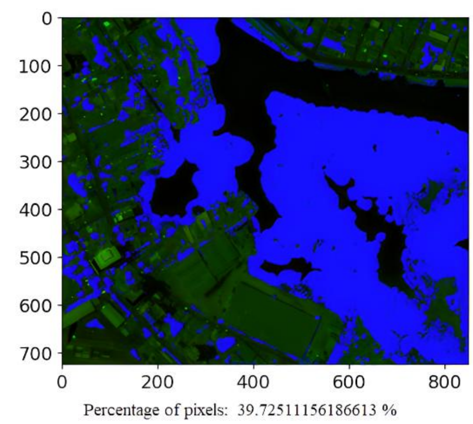

Fig. 10. Vegetation detection map obtained by applying the correlation method to the entire hyperspectral image, used for comparison with the wavelet approach.

The results presented in Fig. 10 and Table II shows that both methods achieve comparable levels of detection accuracy. In particular, the percentage of vegetation pixels detected by the proposed method was 39.72%, which is close to the result obtained with the correlation method, yielding a percentage difference of 3.23%.

TABLE II. VEGETATION DETECTION RESULTS OF THE PROPOSED METHOD VS. CORRELATION METHOD

Method	Vegetation pixels detected	Vegetation percentage
Haar wavelet transform	273488	42.95%
Correlation method	252101	39.72%

The above results indicate that the proposed method provides detection performance comparable to that of the correlation approach, while offering a computationally efficient alternative for environmental monitoring using hyperspectral imagery.

F. Computational Efficiency and Replicability

To evaluate the computational efficiency of the proposed method in comparison with the correlation-based approach, both methods were executed multiple times (20, 40, 60, 80, and 100 executions) on the same reference image region of 50 × 50 pixels with 380 reflectance bands.

The objective of this experiment was to estimate the average execution time as a function of the number of runs for each method, as well as the overall computational behavior under repeated executions. Fig. 11 presents the average execution time curves obtained for both methods.

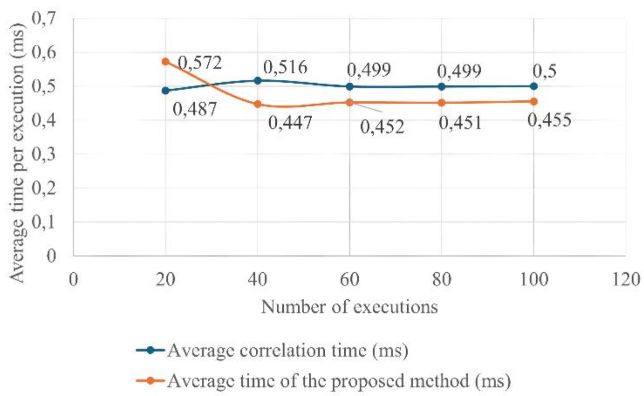

Fig. 11. Average execution time comparison between the proposed wavelet-based method and the correlation-based method for different numbers of executions.

As shown in Fig. 11, the proposed method exhibits a slightly higher average execution time than the correlation method only in the case of 20 executions. For all other evaluated scenarios, the proposed method remains below 0.455 ms and consistently shows lower average execution times as the number of executions increases, indicating better computational efficiency under repeated processing conditions.

It is evident that the average execution time for the correlation method fluctuates around 0.5 ms. By averaging the execution times of both methods and comparing these averages, it is determined that the correlation method is 1.05 times slower than the proposed method, meaning the proposed method is, on average, 4.96% more efficient than the correlation method. While this percentage may be considered small, it could have a greater impact when processing large images, such as those associated with environmental monitoring processes based on hyperspectral imaging.

Centered on the above, Fig. 11 makes it clear that, although the proposed method starts out slightly slower in 20 executions, it becomes increasingly faster as the number of executions increases.

V. Discussion

It is important to highlight that this research contributed a new method for detecting vegetation and materials in hyperspectral images based on the similarity between the approximate and detailed components of the Haar wavelet transform of the characteristic pixel and a given pixel in the image.

From the results obtained during the implementation and evaluation of the method, it was found that, compared to the correlation method, which has been widely disseminated for vegetation detection in hyperspectral images [36], the proposed method was equally effective in detecting vegetation and 4.958% more efficient. This efficiency improvement can result in significant time savings when processing large-volume images, such as those used in environmental monitoring of extensive areas.

From a comparative perspective, the obtained results are consistent with previous studies that have successfully applied similarity-based techniques for vegetation detection in hyperspectral images. Correlation-based approaches have been widely used as reliable baselines in hyperspectral analysis [36], achieving high detection accuracy at the expense of increased computational cost. The comparable detection performance obtained by the proposed method, together with its improved computational efficiency, aligns with recent research efforts focused on reducing processing complexity while preserving spectral discrimination capability.

In contrast to machine learning and deep learning approaches reported in the literature, which often require large annotated datasets and extensive training procedures [34], [35], the proposed method emphasizes interpretability and operational efficiency. Similar trends toward lightweight and data-efficient hyperspectral analysis methods have been reported in studies using dimensionality reduction and transform-based representations [37]–[40], supporting the relevance and practical value of the proposed wavelet-based similarity framework.

From a methodological perspective, in similarity- and threshold-based approaches, increasing the number of sample pixels does not necessarily improve discrimination performance. On the contrary, excessive sampling may lead to saturation of the similarity space and increased overlap between vegetation and non-vegetation classes, making threshold definition more difficult. The sampling strategy adopted in this work was therefore designed to balance representativeness and separability. This explains the stable behavior of the proposed method across different weighting configurations and threshold values, as observed in the experimental results.

Regarding parameter selection, in similarity- and threshold-based detection methods, parameter selection plays a critical role in balancing class separability and robustness. In the proposed approach, the most influential parameters are the weighting coefficients assigned to the approximate and detailed wavelet components, as well as the detection threshold. The results presented in Section IV show that the method exhibits stable behavior within a wide range of weighting configurations for the detailed component (85%–98%), while lower values increase overlap between vegetation and non-vegetation similarity ranges. This indicates that the method is not overly sensitive to minor parameter variations but operates within a clearly defined and interpretable parameter space. Extreme parameter configurations, such as assigning insufficient weight to the detailed component or relaxing the detection threshold, lead to reduced discrimination capability, which is consistent with the nature of similarity- and threshold-based classification methods.

Also, since the proposed method was implemented using open-source libraries and tools, this research holds significant value both academically and commercially, facilitating the adoption and utilization of these technologies in the processing and analysis of spectral images. This not only reduces the costs associated with proprietary tools but also enables the customization of methods and the hybridization of different techniques to meet specific needs.

In this way, the proposed method serves as a key contribution for research centers and universities in developing countries, promoting the replication and expansion of studies involving hyperspectral images. This is particularly relevant as previous research conducted with proprietary tools such as ENVI has demonstrated their utility in this field [41], [42]. The use of open-source alternatives could further enhance accessibility and foster innovation in such studies.

It is important to note that the objective of this study is not to provide a large-scale benchmark across multiple hyperspectral datasets, but to demonstrate the feasibility and effectiveness of a wavelet-based similarity approach for vegetation detection. The use of a single representative hyperspectral scene and a carefully selected set of sample pixels is consistent with threshold-based methods, where the focus is on spectral behavior and separability rather than statistical learning. While additional scenes could further validate robustness across different conditions, the presented results sufficiently support the methodological contribution and computational advantages of the proposed approach.

Although machine learning and deep learning approaches have shown strong performance in hyperspectral vegetation detection, they typically require large annotated datasets, high computational resources, and complex training procedures. The objective of this work is different: to provide a lightweight, interpretable, and computationally efficient alternative suitable for scenarios where labeled data and processing resources are limited. For this reason, the proposed method was compared against the correlation-based approach, which is one of the most widely used similarity-based techniques in hyperspectral analysis and represents a fair baseline in terms of operational complexity.

Regarding noise and illumination variability, the proposed method relies on normalized spectral signatures and on the Haar wavelet transform, which decomposes the signal into approximate (low-frequency) and detailed (high-frequency) components. This decomposition inherently reduces sensitivity to global illumination variations captured in the low-frequency component, while preserving discriminative spectral patterns in the detailed component. Although an explicit noise robustness analysis is beyond the scope of this study, the wavelet-based representation is known to provide increased robustness against high-frequency noise compared to direct spectral similarity measures.

VI. CONCLUSION

Considering that vegetation detection in the domain of hyperspectral images has primarily relied on methods based on correlation and machine learning, which, although accurate, require high computational costs, this study proposed a novel computationally efficient method in the same domain. The proposed method is based on the similarity between the wavelet transform components of the characteristic vegetation pixel and the components of the pixel being analyzed in the image. Given the results obtained in terms of both effectiveness and efficiency, the method can be integrated into academic and commercial contexts within systems for monitoring environmental variables using hyperspectral images.

The results obtained in this research determined that, although the similarity between the approximate and detailed components of the characteristic pixel and the sample pixels showed overlap or proved unsuitable for vegetation detection when considered individually, the similarity percentage based on the weighting of the components is more effective and does not exhibit overlap in the thresholds obtained for vegetation and other materials. The best detection threshold is achieved when the weight of the detailed component is 95%, and the weight of the approximate component is 5%. Thus, the proposed method proves effective through the combined weighting of the similarities, establishing 99.008% as the minimum detection threshold for vegetation. Based on this, the proposed method was successfully applied to the entire reference image, yielding detection results comparable to those of the correlation method.

In line with the above, the deployment of the proposed method on the hyperspectral image of a representative area in the city of Cartagena determined that 42.953% of the pixels correspond to vegetation, with a percentage difference of only 3.23% compared to the correlation method. This demonstrates that the proposed method is a valid and reliable alternative for environmental variable monitoring systems, providing results comparable to existing methods. Furthermore, these results are particularly relevant for continuous monitoring of the areas studied in Cartagena, allowing for an accurate assessment of the impact of urban development on vegetation and, by extension, the environment. This highlights the importance of implementing monitoring tools that enable the understanding and mitigation of the effects of urban growth over time.

In evaluating the computational efficiency of the proposed method compared to the correlation-based method, multiple executions (20, 40, 60, 80, 100) were performed on a region of the reference hyperspectral image measuring 50x50 pixels with 380 reflectance bands. The results showed that, on average, the correlation method is 1.05 times slower than the proposed method, indicating that the proposed method is approximately 4.96% more efficient. While this improvement in efficiency may appear modest at first glance, it becomes significant when processing large-volume hyperspectral images, such as those generated by systems monitoring environmental changes or vegetation shifts through remote sensing, enabling optimization of processing times.

This research demonstrated the relevance and feasibility of using open-source tools and technologies for processing and implementing computational methods for detecting vegetation and other materials in the domain of hyperspectral images. In this context, the spectral library proved useful for accessing the reflectance band data of the reference hyperspectral image. The PyWavelets library enabled the implementation of the proposed method by obtaining the approximate and detailed components of the Haar wavelet transform. The numpy library was essential for accessing and handling hyperspectral image data, facilitating data normalization, image iteration, and the implementation of the correlation method. The pandas library supported the loading of points corresponding to vegetation pixels and other materials. Finally, the matplotlib library was used to generate graphs associated with reflectance curves and the curves corresponding to the components of the characteristic pixel. These technologies can thus be employed to replicate experiments with spectral images in academic and commercial domains, while also enabling the development of new detection methods.

As future work derived from this research, the wavelet transform is intended to be used to obtain a condensed representation of the spectral signature, allowing this summarized signature to be hybridized with other detection methods, such as the Fourier similarity method or the differential similarity method. Additionally, the proposed method will be evaluated for detecting water bodies or other types of materials in various application contexts.

Conflict of Interest

The authors declare no conflict of interest.

Author Contributions

M.O.: conceptualization, writing an original draft, investigation, data curation, reviewing and editing; G.C.: investigation, methodology, reviewing and editing; M.S.: research design, data analysis, funding acquisition, and project administration. All authors have read and agreed to the published version of the manuscript.

Declaration of Generative AI and AI-Assisted Technologies in the Writing Process

During the preparation of this work, the authors used Grammarly and ChatGPT to improve their writing. After using this tool, the authors reviewed and edited the content as needed and took full responsibility for the publication's content.

Acknowledgment

This study is considered as a product within the framework of the project "Development of a comprehensive strategy to reduce the impact on public health and the environment due to the presence of asbestos in the territory of the department of bolívar", funded by the General Royalties System of Colombia (SGR) and identified with code BPIN 2020000100366. This project was carried out by the University of Cartagena, Colombia, and the Asbestos-Free Colombia Foundation.

Finally, the authors of this study would like to thank the University of Cartagena for their support in the development of this research and would like to express their gratitude to Federico Frassy for his support in the management and classification of hyperspectral data, to Aiken Hernando Ortega Heredia, María Angélica Narváez Cuadro, Carlos Andrés Castrillón Ortiz, Michelle Cecilia Montero Acosta, Margareth Peña Castro, Carlos David Arroyo Angulo, and the rest of the research team for logistical support and sample collection in the field. Additionally, the authors extend their thanks to Juan Manuel González from BlackSquare company for assistance in acquiring hyperspectral data and to Sean Fitzgerald for the PLM analysis.

References

[1] J. Sunil and A. Singh, "Evaluation of the Performance of Supervised Classification Alogorithums in Image Classification," Int. J. Curr. Microbiol. Appl. Sci., vol. 8, no. 10, pp. 2634–2643, Oct. 2019, doi: 10.20546/ijcmas.2019.810.304.

[2] J. Awange and J. Kiema, "Fundamentals of Remote Sensing," 2019, pp. 115–123. doi: 10.1007/978-3-030-03017-9_7.

[3] A. A. Misra, "Remote Sensing Fundamentals," in Atlas of Structural Geological and Geomorphological Interpretation of Remote Sensing Images, Wiley, 2022, pp. 7–14. doi: 10.1002/9781119813392.ch1.

[4] A. F. Jiménez-López, M. Jiménez-López, and F. R. Jiménez-López, "Multispectral analysis of vegetation for remote sensing applications," ITECKNE, vol. 12, no. 2, Nov. 2015, doi: 10.15332/iteckne.v12i2.1242.

[5] S. K. Yadav, S. Raj, and S. S. Roy, "Remote sensing technology and its applications," Int. J. Adv. Res. Technol., vol. 2, no. 10, pp. 1–6, 2012.

[6] A. K. Torres Galindo, A. F. Gómez Rivera, and A. F. Jiménez López, "Desarrollo de un sistema multiespectral para aplicaciones en agricultura de precisión usando dispositivos embebidos," Sist. y Telemática, vol. 13, no. 33, pp. 27–44, Jun. 2015, doi: 10.18046/syt.v13i33.2079.

[7] K. Ennouri, M. Ennouri, and M. A. Triki, "Satellite Imagery Used for Analysis of Soil Properties," 2024, pp. 311–334. doi: 10.4018/979-8-3693-6452-9.ch010.

[8] A. Tudor, "Remote sensing in biometeorology," Rev. Air Force Acad., vol. XX, no. 2, pp. 5–14, Feb. 2023, doi: 10.19062/1842-9238.2022.20.2.1.

[9] N. Aburaed, M. Q. Alkhatib, S. Marshall, J. Zabalza, and H. Al Ahmad, "A Review of Spatial Enhancement of Hyperspectral Remote Sensing Imaging Techniques," IEEE J. Sel. Top. Appl. Earth Obs. Remote Sens., vol. 16, pp. 2275–2300, 2023, doi: 10.1109/JSTARS.2023.3242048.

[10] M. J. Khan, H. S. Khan, A. Yousaf, K. Khurshid, and A. Abbas, "Modern Trends in Hyperspectral Image Analysis: A Review," IEEE Access, vol. 6, pp. 14118–14129, 2018, doi: 10.1109/ACCESS.2018.2812999.

[11] Y. Gu et al., "Multimodal hyperspectral remote sensing: an overview and perspective," Sci. China Inf. Sci., vol. 64, no. 2, p. 121301, Feb. 2021, doi: 10.1007/s11432-020-3084-1.

[12] A. S. Gautam, "A Comprehensive Literature Review on Hyperspectral Remote Sensing Techniques and Applications," INTERANTIONAL J. Sci. Res. Eng. Manag., vol. 08, no. 06, pp. 1–5, Jun. 2024, doi: 10.55041/IJSREM35929.

[13] L. Zhang and Y. Zhong, "Analysis of Hyperspectral Remote Sensing Images," in Geospatial Technology for Earth Observation, Boston, MA: Springer US, 2010, pp. 235–269. doi: 10.1007/978-1-4419-0050-0_9.

[14] C. Cucci, J. K. Delaney, and M. Picollo, "Reflectance Hyperspectral Imaging for Investigation of Works of Art: Old Master Paintings and Illuminated Manuscripts," Acc. Chem. Res., vol. 49, no. 10, pp. 2070–2079, Oct. 2016, doi: 10.1021/acs.accounts.6b00048.

[15] M. Caccia, S. Caglio, A. Galli, M. Interlenghi, I. Castiglioni, and M. Martini, "Applying Hyperspectral Reflectance Imaging to Investigate the Palettes and the Techniques of Painters," J. Vis. Exp., no. 172, Jun. 2021, doi: 10.3791/62202.

[16] L. Gao and R. T. Smith, "Optical hyperspectral imaging in microscopy and spectroscopy - a review of data acquisition," J. Biophotonics, vol. 8, no. 6, pp. 441–456, Jun. 2015, doi: 10.1002/jbio.201400051.

[17] J. Burger and A. Gowen, "Data handling in hyperspectral image analysis," Chemom. Intell. Lab. Syst., vol. 108, no. 1, pp. 13–22, Aug. 2011, doi: 10.1016/j.chemolab.2011.04.001.

[18] A. Ramírez et al., "Sistema de visión hiperespectral para el estudio de especies arbóreas tropicales," Rev. Tecnol. en Marcha, Jun. 2022, doi: 10.18845/tm.v35i6.6239.

[19] A. Riaza, E. García-Meléndez, V. Carrère, and A. Mueller, "Cartografía de sales marinas y fluviales en estuarios receptores de aguas ácidas con imágenes hiperespectrales Hyperion (Marismas del río Odiel, Huelva)," Rev. Teledetección, no. 41, p. 1, Jun. 2014, doi: 10.4995/raet.2014.2255.

[20] W. A. Nugraha, P. Wicaksono, and S. Arjasakusuma, "Vegetation Change Detection Analysis Using Multi-sensor Hyperspectral Imagery," J. Geogr. (Geografi Lingkung. Lahan Basah), vol. 5, no. 1, p. 9, Jul. 2024, doi: 10.20527/jgp.v5i1.11709.

[21] G. Nico, M. Monaco, O. Masci, and M. G. C. A. Cimino, "High Resolution Mapping of Vegetation Biodiversity by Hyperspectral Images and Convolutional Autoencoders," in IGARSS 2024 - 2024 IEEE International Geoscience and Remote Sensing Symposium, Jul. 2024, pp. 2247–2250. doi: 10.1109/IGARSS53475.2024.10640541.

[22] H. Chen, "Microscopic Hyperspectral Image Analysis via Deep Learning," Griffith University, 2020. doi: 10.25904/1912/3909.

[23] J. Nalepa, "Recent Advances in Multi- and Hyperspectral Image Analysis," Sensors, vol. 21, no. 18, p. 6002, Sep. 2021, doi: 10.3390/s21186002.

[24] Y. E. García-Vera, A. Polochè-Arango, C. A. Mendivelso-Fajardo, and F. J. Gutiérrez-Bernal, "Hyperspectral Image Analysis and Machine Learning Techniques for Crop Disease Detection and Identification: A Review," Sustain., vol. 16, no. 14, 2024, doi: 10.3390/su16146064.

[25] S. Mahesh, D. S. Jayas, J. Paliwal, and N. D. G. White, "Hyperspectral imaging to classify and monitor quality of agricultural materials," J. Stored Prod. Res., vol. 61, pp. 17–26, Mar. 2015, doi: 10.1016/j.jspr.2015.01.006.

[26] C. Wang et al., "A review of deep learning used in the hyperspectral image analysis for agriculture," Artif. Intell. Rev., vol. 54, no. 7, pp. 5205–5253, Oct. 2021, doi: 10.1007/s10462-021-10018-y.

[27] J. A. Guzman-Alvarez, M. González-Zuñiga, J. A. Sandoval Fernandez, and J. C. Calvo-Alvarado, "Uso de sensores remotos en la agricultura: aplicaciones en el cultivo del banano," Agron. Mesoam., p. 48279, Aug. 2022, doi: 10.15517/am.v33i3.48279.

[28] M. T. Ahmed, A. Villordon, and M. Kamruzzaman, "Comparative analysis of hyperspectral Image reconstruction using deep learning for agricultural and biological applications," Results Eng., vol. 23, p. 102623, Sep. 2024, doi: 10.1016/j.rineng.2024.102623.

[29] B. Jia et al., "Essential processing methods of hyperspectral images of agricultural and food products," Chemom. Intell. Lab. Syst., vol. 198, p. 103936, Mar. 2020, doi: 10.1016/j.chemolab.2020.103936.

[30] B. Lu, P. Dao, J. Liu, Y. He, and J. Shang, "Recent Advances of Hyperspectral Imaging Technology and Applications in Agriculture," Remote Sens., vol. 12, no. 16, p. 2659, Aug. 2020, doi: 10.3390/rs12162659.

[31] B. Wang et al., "The Applications of Hyperspectral Imaging Technology for Agricultural Products Quality Analysis: A Review," Food Rev. Int., vol. 39, no. 2, pp. 1043–1062, Feb. 2023, doi: 10.1080/87559129.2021.1929297.

[32] A. Plaza et al., "Recent advances in techniques for hyperspectral image processing," Remote Sens. Environ., vol. 113, pp. S110–S122, Sep. 2009, doi: 10.1016/j.rse.2007.07.028.

[33] B. Mohan and A. Porwal, "Hyperspectral Image Processing and Analysis," Curr. Sci., vol. 108, pp. 833–841, 2015, doi: https://doi.org/10.18520/CS/V108/I5/833-841.

[34] S. Li, W. Song, L. Fang, Y. Chen, P. Ghamisi, and J. A. Benediktsson, "Deep Learning for Hyperspectral Image Classification: An Overview," IEEE Trans. Geosci. Remote Sens., vol. 57, no. 9, pp. 6690–6709, Sep. 2019, doi: 10.1109/TGRS.2019.2907932.

[35] X. Yang, Y. Ye, X. Li, R. Y. K. Lau, X. Zhang, and X. Huang, "Hyperspectral Image Classification With Deep Learning Models," IEEE Trans. Geosci. Remote Sens., vol. 56, no. 9, pp. 5408–5423, Sep. 2018, doi: 10.1109/TGRS.2018.2815613.

[36] G. E. Chanchí Golondrino, M. A. Ospina Alarcón, and M. Saba, "Vegetation Identification in Hyperspectral Images Using Distance/Correlation Metrics," Atmosphere (Basel)., vol. 14, no. 7, p. 1148, Jul. 2023, doi: 10.3390/atmos14071148.

[37] B. Dastourian, E. Dastourian, S. Dastourian, and O. Mahnaie, "Discrete Wavelet Transforms Of Haar's Wavelet," Int. J. Sci. Technol. Res., vol. 3, pp. 247–251, 2014.

[38] D. B. Percival and A. T. Walden, "The Discrete Wavelet Transform," in Wavelet Methods for Time SeriesAnalysis, Cambridge: Cambridge University Press, 2000, pp. 56–158. doi: 10.1017/CBO9780511841040.005.

[39] H. Husain and A. Amran, "Forecasting Time Series Data Using Haar Discrete Wavelet Transformation," J. Mat. Stat. dan Komputasi, vol. 19, no. 3, pp. 484–497, May 2023, doi: 10.20956/j.v19i3.24807.

[40] S. Gurumoorthy, N. Babu Muppalaneni, and G. Sandhya Kumari, "EEG Signal Denoising Using Haar Transform and Maximal Overlap Discrete Wavelet Transform (MODWT) for the Finding of Epilepsy," in Epilepsy - Update on Classification, Etiologies, Instrumental Diagnosis and Treatment, IntechOpen, 2021. doi: 10.5772/intechopen.93180.

[41] F. Salem, M. Kafatos, T. El-Ghazawi, R. Gomez, and R. Yang, "Hyperspectral image assessment of oil-contaminated wetland," Int. J. Remote Sens., vol. 26, no. 4, pp. 811–821, Feb. 2005, doi: 10.1080/01431160512331316883.

[42] D. W. y Yanbo Huang y Zhao Chunjiang y Wang Xiu, "Identificación de plántulas de col y malezas mediante imágenes hiperespectrales," Int. J. Agric. Biol. Eng., vol. 8, pp. 65–72, 2015, doi: 10.25165/IJABE.V8I5.1492.